Evolution of short-range order and its effects on the plastic deformation behavior of single crystals of the equiatomic Cr-Co-Ni medium-entropy alloy

AUTHOR(S):

Li, Le; Chen, Zhenghao; Kuroiwa, Shogo; Ito, Mitsuhiro; Yuge, Koretaka; Kishida, Kyosuke; Tanimoto, Hisanori; Yu, Yue; Inui, Haruyuki; George, Easo P.

CITATION:

Li, Le ...[et al]. Evolution of short-range order and its effects on the plastic deformation behavior of single crystals of the equiatomic Cr-Co-Ni medium-entropy alloy. Acta Materialia 2023, 243: 118537.

ISSUE DATE:

2023-01-15

URL:

http://hdl.handle.net/2433/282860

Acta Materialia 243 (2023) 118537

Contents lists available at ScienceDirect

Acta Materialia

journal homepage: www.elsevier.com/locate/actamat

Full length article

Evolution of short-range order and its effects on the plastic deformation behavior of single crystals of the equiatomic Cr-Co-Ni medium-entropy alloy

Le Li [a], Zhenghao Chen [a,b], Shogo Kuroiwa [a], Mitsuhiro Ito [a], Koretaka Yuge [a], Kyosuke Kishida [a,b,*], Hisanori Tanimoto [c], Yue Yu [c], Haruyuki Inui [a,b], Easo P. George [d,e]

[a] Department of Materials Science and Engineering, Kyoto University, Kyoto 606-8501, Japan
[b] Center for Elements Strategy Initiative for Structure Materials (ESISM), Kyoto University, Kyoto 606-8501, Japan
[c] Degree Programs in Pure and Applied Sciences, Graduate School of Science and Technology, University of Tsukuba, Tsukuba 305-8573, Japan
[d] Materials Science and Engineering Department, University of Tennessee, Knoxville, TN 37996, USA
[e] Institute for Materials, Ruhr University Bochum, Bochum 44801, Germany

ARTICLE INFO

Keywords:
High entropy alloys
Single crystals
Mechanical properties
Critical resolved shear stress
Short-range ordering

ABSTRACT

Short-range ordering (SRO), its evolution in the equiatomic Cr-Co-Ni medium-entropy alloy (MEA), and its effects on mechanical properties were investigated by, respectively, electrical resistivity measurements and tension and compression tests on single crystal specimens at room temperature and liquid nitrogen temperature. SRO below 973 K can be monitored by changes in electrical resistivity, which increases gradually with time to a saturation value during isothermal annealing in the temperature range of 673–973 K. While the time required to reach saturation is shorter at higher temperatures, the saturation resistivity is higher at lower temperatures, indicating a higher degree of SRO at lower temperature although it takes longer to reach saturation because of slower kinetics. No significant change in the plastic deformation behavior is found at room temperature and 77 K for different degrees of SRO. The yield stress as well as the slip localization behavior are basically the same after SRO, and the magnitude of yield drop does not correlate with the degree of SRO. Tensile stress-strain curves are not much affected by SRO up to high strain levels, resulting in identical shear stresses for the onset of deformation twinning at room temperature regardless of the degree of SRO. The dislocation structure, variations in dislocation dissociation width, and stacking fault energy are all essentially unchanged.

1. Introduction

In recent years, a new class of alloys called high- and medium-entropy alloys (HEAs and MEAs) have attracted the attention of a tremendous number of materials scientists all over the world. Research on HEAs and MEAs has thus become one of the most active areas in materials science today with many review papers published recently [1–8]. This stems from the fact that some solid-solution HEAs and MEAs exhibit extraordinary mechanical properties such as simultaneous achievement of high strength and high ductility, although such extraordinary mechanical properties are not necessarily achieved by all HEAs and MEAs [2,3]. Severely distorted crystal lattices of HEAs and MEAs, which arise from varying atomic sizes of the constituent elements, are thought to play a decisive role in the extraordinary mechanical properties [9,10]. Many early investigations assumed a completely random atomic structure in HEAs and MEAs. In recent years, however, short-range ordering (SRO) that may occur as a result of the mixing enthalpy contribution to the Gibbs free energy [11], has been a focus of intensive studies in HEAs and MEAs [4,12]. Some researchers foresee that further improvement of mechanical properties may be possible by tuning the degree of SRO in HEAs and MEAs [13,14].

SRO is not restricted to HEAs and MEAs. Many conventional alloys, even simple binaries, are known to exhibit non-random atomic structures accompanied by SRO or short-range clustering (SRC) of the constituent elements with the degree of SRO and SRC varying depending on heat treatment [15–22]. SRO in conventional alloys is demonstrated by x-ray, neutron or electron diffraction [23,24], or by electrical resistivity and specific heat measurements [25,26]. In the last several decades,

* Corresponding author at: Department of Materials Science and Engineering, Kyoto University, Kyoto 606-8501, Japan.
E-mail address: kishida.kyosuke.6w@kyoto-u.ac.jp (K. Kishida).

https://doi.org/10.1016/j.actamat.2022.118537
Received 13 June 2022; Received in revised form 16 November 2022; Accepted 17 November 2022
Available online 19 November 2022

effects of SRO on strength have been the subject of many investigations, especially in solid-solution alloys with the face-centered cubic (FCC) structure. Many of these investigations employed one (or some) of the above-mentioned methods (with electrical resistivity being the most frequently employed [19,27], sometimes combined with x-ray, neutron or electron diffraction [22,28,29]) to monitor the evolution of SRO and to subsequently correlate it with strength. In the early days, simple theories were proposed to account for SRO strengthening that scaled with γ_{db}/b (γ_{db}: SRO domain-boundary energy, b: the magnitude of dislocation Burgers vector) on the assumption that the interaction of SRO domain-boundaries and gliding dislocations contributes to strengthening [30,31]. However, Cohen and Fine [32] later concluded that the overall alloy strength is not affected significantly by SRO; rather, they argued, the effects of SRO should be manifested as a yield drop in the stress-strain curve with the magnitude of the yield drop depending on the degree of SRO. This conclusion was based on the consideration that the initial high resistance to dislocation motion arising from SRO is quickly lowered by the passage of the first several dislocations that destroy SRO on the slip plane; subsequent dislocations moving on the same slip plane then experience less resistance resulting in coarse (localized) slip. Consistent with the above notion of Cohen and Fine, Scattergood and Bever [17] reported that, while the magnitude of the yield-drop correlates well with the degree of SRO developed, all other mechanical properties including yield strength do not correlate with SRO in Cu-Al polycrystals. However, many other experimental observations that contradicted Cohen and Fine [32] have been reported from time to time. For example, Büttner and Nembach [18] and Svitak and Asimow [33] reported that neither the yield strength nor the yield-drop correlate with the degree of SRO in Cu-Au and Ag-Au polycrystals, respectively. On top of that, Büttner and Nembach [18] reported that the yield strength of Cu-Au polycrystals reached a minimum when the degree of SRO reached a maximum. While this contradicted the general belief that strength increases with the degree of SRO developed [30,31] it was subsequently shown to be consistent with elasticity calculations of dislocations in Ag-Al alloys by Patu and Arsenault [34]. Thus, when the entire weight of the evidence is considered, it becomes clear that there is a lack of agreement on how strength varies with SRO, even in conventional alloys.

SRO has been reported in the equiatomic Cr-Co-Ni MEA [11,35,36], as well as in FCC HEAs of the Cr-Mn-Fe-Co-Ni system and its FCC MEA subsystems [13,35,37–47]. Among these, the equiatomic Cr-Co-Ni MEA is the most extensively studied. It is worth noting, however, that SRO in the equiatomic Cr-Co-Ni MEA, as well its effects on mechanical properties, are mostly investigated by theoretical calculations based on density-functional theory (DFT) and simulations [13,14,39,41,44]. A substantial increase in strength associated with SRO has been suggested by DFT calculations due to local fluctuations in stacking fault (SF) energy arising from the non-random atomic structure [13,14,39,41,44]. On the other hand, experimental efforts to demonstrate the presence of SRO in the equiatomic Cr-Co-Ni MEA and to elucidate its effects on mechanical properties are rather limited [43,48]. This is due mainly to the difficulty in experimentally proving the presence of SRO by x-ray and electron diffraction because of the very small difference in atomic scattering factor of the constituent elements, Cr, Co and Ni over a wide range of scattering angles (Fig. S1). Although there are some reports of SRO based on electron diffraction and diffraction imaging [37,43], the evidence is not unambiguous. Furthermore, different experimental investigators have drawn opposing conclusions on the effects of SRO on mechanical properties [43,48]. Zhang et al. [43] reported remarkable strengthening (yield strength increase of 25%) due to SRO in equiatomic Cr-Co-Ni MEA polycrystals after annealing at 1273 K followed by furnace cooling, while Inoue et al. [48] reported no measurable effect of SRO on the yield strength of equiatomic Cr-Co-Ni MEA polycrystals after annealing at 973 K for 384 h followed by water quenching. Note that neither of these studies quantified the degree of SRO responsible for their respective mechanical properties. Therefore, more work is needed to explore the effect of SRO on the strength of the equiatomic Cr-Co-Ni MEA.

In the present study, we investigate (1) the evolution of SRO in the equiatomic Cr-Co-Ni MEA by monitoring changes in electrical resistivity, and (2) the effect of the degree of SRO on the mechanical properties of single crystals of the equiatomic Cr-Co-Ni MEA in tension and in compression at room temperature and liquid-nitrogen temperature. We investigate in particular how critical resolved shear stress (CRSS) for {111}<110> slip, onset shear stress for {111}<112> twinning, yield drop, slip localization as well as stacking fault (SF) energy are affected by the development of SRO by monitoring electrical resistivity changes.

2. Experimental procedures

Ingots of the equiatomic Cr-Co-Ni alloy were prepared by arc-melting high-purity (>99.9%) Cr, Co and Ni in an argon atmosphere. Some of these ingots were homogenized at 1473 K for 168 h. Rectangular parallelepiped specimens were cut from the homogenized ingots, cold rolled to 50% thickness reduction and then recrystallized at 1273 K for 2 h, followed by water quenching. Slices with dimensions 50 × 2 × 0.5 mm^3 were cut from the recrystallized ingots and then mechanically polished with 1 μm diamond paste. Electrical resistivity measurements were performed on these slices by the four-terminals method at room temperature to monitor the evolution of short-range order after isothermal annealing at various temperatures (573 to 973 K). Some of the arc-melted ingots were used to grow single crystals of the Cr-Co-Ni MEA with an optical floating-zone furnace in flowing Ar gas at a growth rate of 10 mm/h. The single crystals were homogenized at 1473 K for 168 h followed by water quenching. Then, they were annealed at 573–873 K for 168–504 h followed by water quenching. After determining crystallographic orientations by the x-ray back-reflection Laue method, single crystal specimens with the $[\bar{1}23]$ loading-axis direction were cut by spark-machining for compressive and tensile tests, measuring 2 × 2 × 5 mm^3 in the gage section. Specimen surfaces were polished first mechanically and then electrolytically with a solution of perchloric acid, n-butanol and methanol (7.5: 29: 63.5 by volume) to obtain a mirror finish. Compression and tensile tests were conducted on an Instron-type testing machine at room temperature (in ambient air) and at 77 K (with the specimen immersed in liquid nitrogen) at an engineering strain rate of 1×10^{-4} s^{-1}. For some specimens tested in tension at room temperature, changes in electrical resistivity during deformation were monitored by interrupting tensile tests at various stages of deformation. Deformation markings on specimen surfaces were examined by optical microscopy, scanning electron microscopy (SEM; JEOL JEM-7001FA operated at 20 kV) and atomic force microscopy (AFM; Shimadzu SPM-9600). Dislocation structures were examined by transmission electron microscopy (TEM) with a JEOL JEM-2000FX electron microscope operated at 200 kV. Thin foils for TEM observations were prepared by electro-polishing in a solution of nitric acid, ethylene glycol and methanol (2: 5: 20 by volume).

TEM and scanning transmission electron microscopy (STEM; JEOL JEM-ARM200F electron microscopes operated at 200 kV) as well as synchrotron x-ray diffraction (SPring-8, BL02B1 beam line) were further utilized to gain information about atomic arrangements in single-crystal specimens subjected to various heat-treatments designed to suppress or promote short-range ordering.

3. Results

3.1. Electrical resistivity

Equiatomic Cr-Co-Ni polycrystals were first quenched from 1473 K and then isothermally annealed for various times at temperatures ranging from 573 to 973 K. Their normalized room-temperature

electrical resistivities (ρ/ρ_0) are plotted in Fig. 1(a) as a function of annealing time, where $\rho_0 = 0.028161 \pm 0.00006\ \Omega$ is the electrical resistivity of specimens quenched from 1473 K. While no significant change in electrical resistivity occurs during isothermal annealing at 573 K, it increases gradually and reaches a saturation value at the other temperatures investigated, 673–973 K. The time required to reach the saturation value is shorter at higher temperatures, but the saturation value is higher at lower temperatures. Saturation already occurs after 0.05 h at 973 K whereas the resistivity (and implied SRO) continues to increase even after 500 h at 673 K. This behavior is consistent with SRO evolution in many FCC alloys such as Cu-Au [18], Ni-Cr [49] and Cu-Pd [50] alloys. For the equiatomic Cr-Co-Ni polycrystals, the largest saturation value obtained at 673 K is greater than ρ_0 by ~4.8%. This increment in electrical resistivity associated with SRO is comparable to those reported for Ni-Cr alloys (~3% at 673 K) [49] and Cu-Pd alloys (~7% at 523 K) [50] but is larger than that reported for Cu-Au alloys (~1% at 423 K) [18]. It is important to note that the increase in electrical resistivity after low-temperature (673–973 K) anneals is fully reversible, that is, the original value can be obtained by annealing at 1473 K followed by quenching. This reversibility strongly suggests that the formation of SRO indeed occurs by low-temperature annealing and that electrical resistivity is a good way to monitor changes in the degree of SRO.

We fit the time-dependent variation of electrical resistivity after isothermal annealing at 673, 773 and 873 K with the following equation,

$$\rho(t)/\rho_0 = 1 + \delta\{1 - \exp(-t/\beta)\} \quad (1)$$

where t is annealing time and δ and β are constants depending on the annealing temperature. The results of fitting are tabulated in Table 1. When the increase in resistivity reflects the volume of SRO formed and the constant δ represents the fractional volume at saturation, Eq. (1) can be regarded as an Avrami-type equation for the time dependence of SRO with Avrami index $n = 1$ (needle-like growth). On the assumption that the behavior shown in Fig. 1(a) is controlled by atomic diffusion, the temperature dependence of β can be expressed with the following Arrhenius-type equation,

$$\beta = \beta_0 \exp(E/RT) \quad (2)$$

where β_0 is a pre-exponential factor, R the gas constant, T the absolute temperature and E the activation energy. The natural logarithm of β is plotted in Fig. 1(b) as a function of inverse temperature. The activation energy and pre-exponential factor deduced from Fig. 1(b) are $E = 194 \pm 27$ kJ/mol and $\beta_0 = 2.85 \times 10^{-10\pm1.7}$ s. The activation energy obtained from Fig. 1(b) is smaller than those (250–310 kJ/mol [51,52]) usually reported for atomic diffusion in HEAs and MEAs of the Cr-Mn-Fe-Co-Ni system. However, a recent tracer diffusion experiment indicates that atomic diffusion of Co and Ni below 1100 K occurs faster with smaller activation energies (206 and 185 kJ/mol) than what is expected from the extrapolation from high temperatures due presumably to the tendency for SRO formation in a Cr-Mn-Fe-Co-Ni alloy [53]. We suspect a similar diffusion behavior occurs also in the Cr-Co-Ni alloys at low temperatures due to SRO.

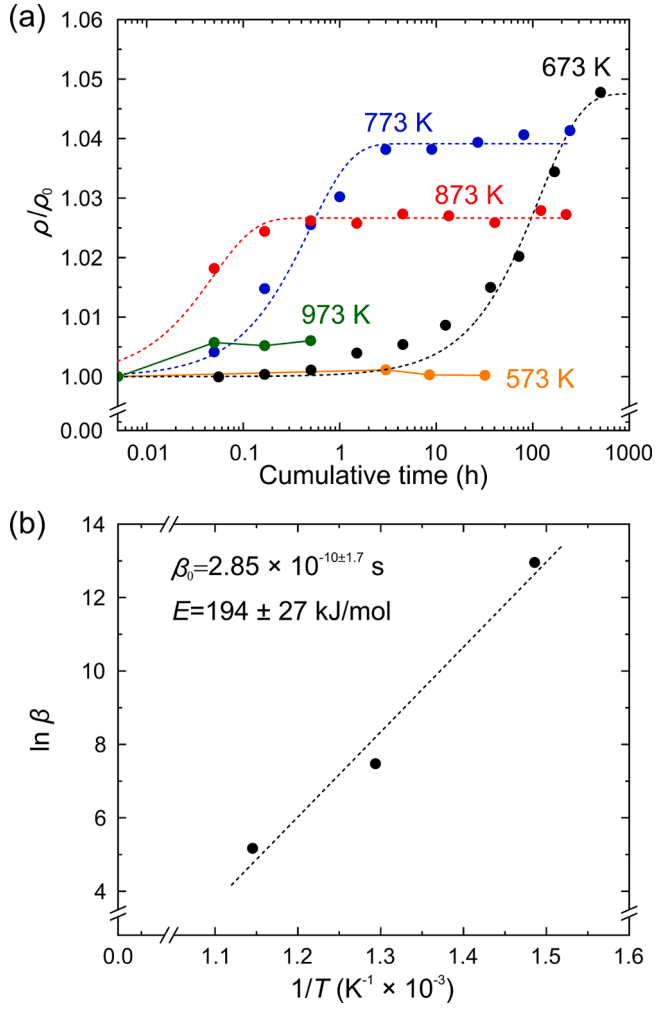

Fig. 1. (a) Variations in electrical resistivity of the equiatomic Cr-Co-Ni polycrystals quenched from 1473 K during isothermal annealing at various temperatures in a range from 573 to 973 K. (b) Arrhenius plot of relaxation time β for resistivity change by isothermal annealing.

3.2. Electron and X-ray diffraction

Selected-area electron diffraction (SAED) patterns with the [111] and [112] incidences taken from the single crystals water-quenched from 1473 K and subsequently annealed at 773 K for 168 h are shown in Fig. 2(a), (b) and Fig. 3(a), (b), respectively. We selected these two specimens, based on Fig. 1(a), as representatives of the highest and lowest degrees of SRO, respectively. The specimen annealed at 773 K for 168 h exhibits a greater than 4% increase in electrical resistivity, which is the highest among the curves in Fig. 1(a). In FCC solid-solutions, short-range ordering of the $L1_2$- or $L1_0$-type has been theoretically predicted [40,54,55] and experimentally verified [22,29,40,48] in the Cr-Co-Ni MEA and its related alloys. However, in the present study, no diffuse intensity indicative of SRO of the $L1_2$- or $L1_0$-type is observed at their superlattice reflection positions (for example at $1\bar{1}0$-type positions) in the SAED patterns (Figs. 2(a), (b) and 3(a), (b)), as seen in the intensity profile between the transmitted beam and $2\bar{2}0$ reflection for both [111] incidence (Figs. 2(c) and 3(c)) and [112] incidence (Figs. 2(d) and 3(d)). This, however, does not rule out SRO of the $L1_2$- or $L1_0$-type in the Cr-Co-Ni MEA, in view of the very small difference in atomic scattering factor of the constituent elements, Cr, Co and Ni. Instead, some diffuse intensity is observed at positions of 1/3{422} and 1/2{113} respectively in the SAED patterns for [111] and [112] incidences, as marked with dotted circles in Figs. 2(a), (b) and 3(a), (b). However, no significant difference in the intensity of such diffuse scattering is observed between

Table 1
Fitting parameters used to describe the Eqs. (1) and (2).

Annealing temperature (K)	δ	β	β_0	E (kJ/mol)
673	0.04753	4.23×10^5	$2.85 \times 10^{10\pm1.7}$	194±27
773	0.03914	1.76×10^3		
873	0.02663	1.75×10^2		

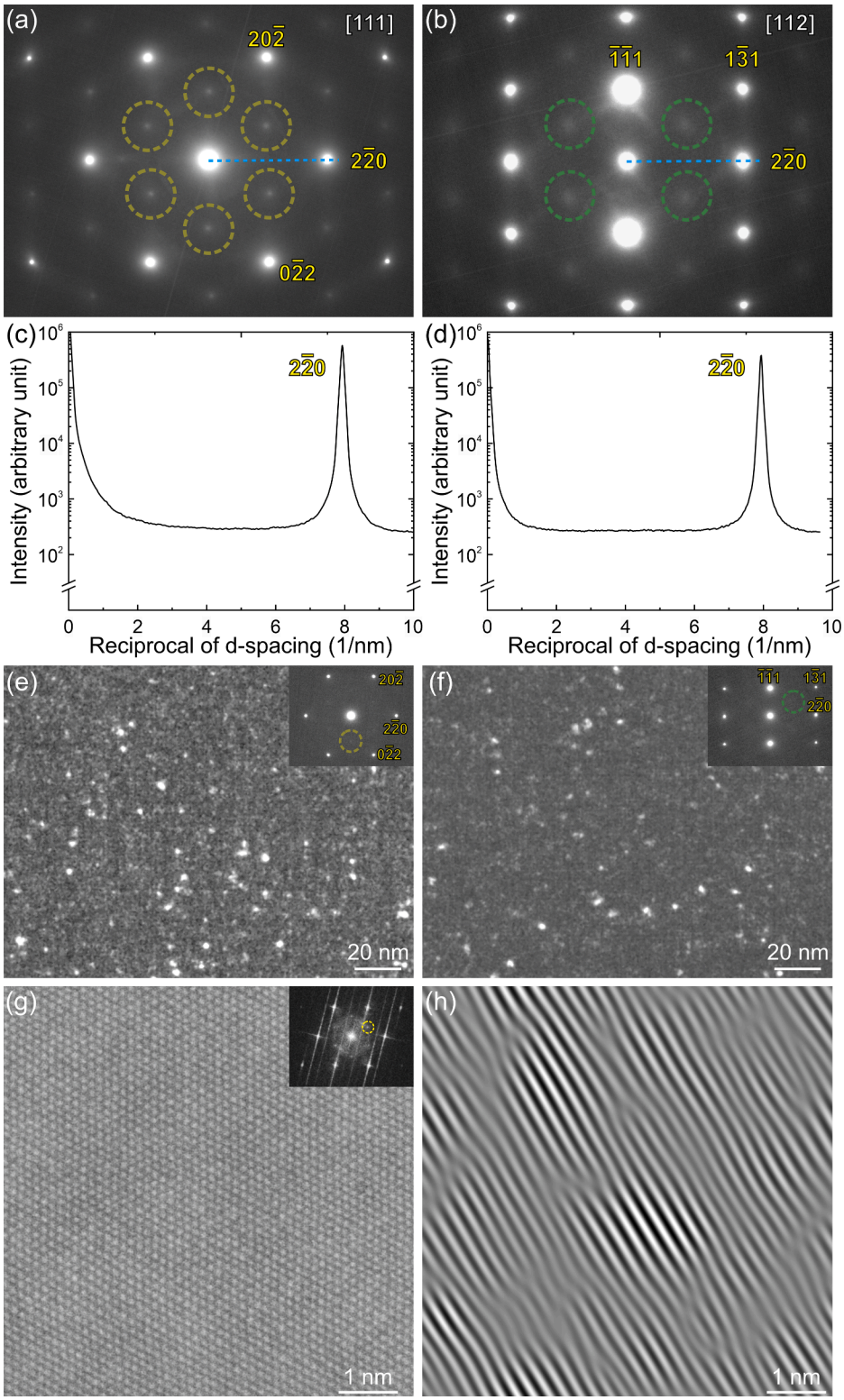

Fig. 2. SAED patterns with the (a) [111] and (b) [112] incidences taken from the single crystals water-quenched from 1473 K. Intensity profile along a line between the transmitted beam and $2\bar{2}0$ reflection in SAED patterns with (c) [111] and (d) [112] incidences. Dark-field images formed by setting an objective aperture at a position of (e) 1/3{422} and (f) 1/2{113} (as shown in the inset SAED patterns). (g) Atomic-resolution HAADF-STEM image taken along [111] with FFT diagram (inset). (h) Inverse FFT image formed with the diffuse intensities at 1/3{422} position in the FFT diagram.

the two specimens in which significantly different degrees of SRO are expected. Many previous studies on SRO in FCC solid-solution alloys assume that the diffuse intensity at positions of 1/3{422} and 1/2{113} is an indication of the occurrence of SRO [37,45,56–58], although this has never been verified. Dark-field imaging by setting an objective aperture at a position of 1/3{422} or 1/2{113} reveals some small bright regions with sizes of 1–2 nm in diameter, however, without any significant difference between the two specimens (Figs. 2(e), (f) and 3(e), (f)).

Fig. 2(g) and Fig. 3(g) show, respectively, atomic-resolution high-angle annular dark-field (HAADF)-STEM images taken along [111] for single crystals water-quenched from 1473 K and subsequently annealed at 773 K for 168 h. Although the intensity of each of the imaged atomic columns is known to be proportional to the square of the averaged atomic number of constituent elements in the relevant column, no particular atomic arrangement that may be related to SRO is observed in

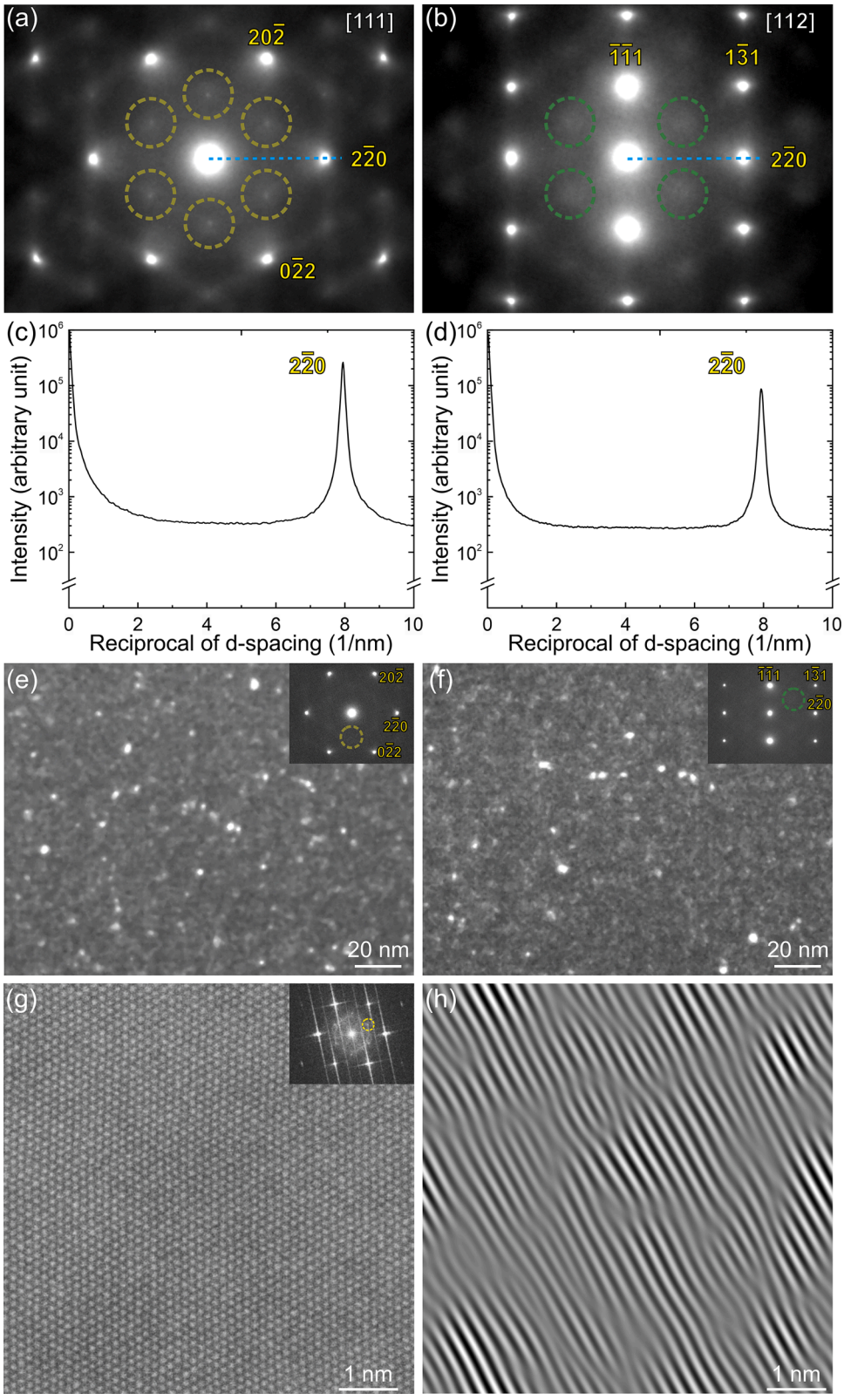

Fig. 3. SAED patterns with the (a) [111] and (b) [112] incidences taken from the single crystals subsequently annealed at 773 K for 168 h after water-quenching from 1473 K. Intensity profile along a line between the transmitted beam and $2\bar{2}0$ reflection in SAED patterns with (c) [111] and (d) [112] incidences. Dark-field images formed by setting an objective aperture at a position of (e) 1/3{422} and (f) 1/2{113} (as shown in the inset SAED patterns). (g) Atomic-resolution HAADF-STEM image taken along [111] with FFT diagram (inset). (h) Inverse FFT image formed with the diffuse intensities at 1/3{422} position in the FFT diagram.

either specimen. This is understandable given the small difference in atomic numbers of Cr, Co and Ni. Fast Fourier transforms (FFT) of these HAADF-STEM images reveal diffuse intensities at 1/3{422} positions (insets in Figs. 2(g) and 3(g)), as in the SAED patterns of Figs. 2(a) and 3(a). Inverse FFT images formed with these diffuse intensities at 1/3{422} positions exhibit scattered small bright regions with sizes of 1~2 nm in diameter but, again, without any significant difference between the two specimens (Figs. 2(e), (f) and 3(e), (f)). Zhou et al. [37] claimed that the occurrence of 1/2{311} diffuse intensity in the [112] SAED is clear evidence of SRO in Cr-Co-Ni subjected to annealing at 873 K for 1 h and that the small regions revealed by inverse FFT imaging with such diffuse scattering correspond to short-range ordered domains. Similar

claims were made also for Al-Cr-Co-Ni [58], Cr-Mn-Fe-Co [45] and V-Co-Ni [57] MEAs. However, neither the diffuse intensities at positions of 1/3{422} and 1/2{113} nor the sizes of the small regions revealed by dark-field TEM imaging and by inverse FFT of atomic-resolution HAADF-STEM images (presumed to be short-range ordered domains) vary when the electrical resistivity changes, i.e., they do not depend on the degree of SRO, as seen in Figs. 2 and 3. This calls into question the correlation between diffuse intensities at positions of 1/3{422} and 1/2{113} in diffraction patterns and SRO in the Cr-Co-Ni MEA.

Indeed, even in Cu, a pure FCC element, diffuse intensity is observed at positions of 1/3{422} and 1/2{113} in SAED patterns with the [111] and [112] incidences (Fig. S2(a) and (b)) and dark-field imaging with these diffuse intensities reveals some small bright regions (Fig. S2(e) and (f)) not unlike those seen in the Cr-Co-Ni MEA. There is a long history of these diffuse intensities being attributed to factors other than SRO, such as thin film effects ({111} relrod spiking from the first-order Laue zone (FOLZ) into the zero-th layer), surface steps, incorporation of defects on {111} (stacking faults, twins and HCP layers) and so on [59–65]. In view of the very small difference in atomic scattering factor of the constituent elements of the Cr-Co-Ni MEA, we strongly suspect that the occurrence of diffuse scattering at 1/3{422} and 1/2{113} positions in the SAED patterns in the Cr-Co-Ni MEA is due mainly to thin film effects ({111} relrod spiking) and surface steps rather than SRO. In fact, no diffuse intensities are present at these positions in the synchrotron x-ray diffraction patterns (Fig. S3). This clearly indicates that the development of SRO in the Cr-Co-Ni MEA cannot be monitored by simple x-ray and electron diffraction experiments.

3.3. Mechanical properties

3.3.1. Yield stress in compression and tension

We investigated how the deformation behavior of single crystals of the equiatomic Cr-Co-Ni alloys changes with electrical resistivity (i.e., the degree of SRO) upon annealing. Fig. 4 shows the temperature and time dependence of the critical resolved shear stress (CRSS) for (111) slip. Values of CRSS were calculated from the yield stresses defined as the 0.2% flow stress multiplied by the Schmid factor (0.467) of the [$\bar{1}$23] orientation. CRSS values for (111) slip obtained at room temperature in compression and tension, and at 77 K in compression are plotted in Fig. 4 (a) as a function of annealing temperature (after first annealing at 1473 K for 168 h and water quenching). All these specimens were annealed at the indicated temperatures for the same length of time (168 h), followed by water-quenching prior to mechanical testing. The CRSS values at room temperature and 77 K (65 and 133 MPa, respectively [66]) obtained previously in compression for specimens quenched from 1473 K after annealing for 168 h are indicated with a dotted line in Fig. 4(a). After 168 h, the degree of SRO is expected to be the largest for the 773 K anneal, followed by the 673 and 873 K anneals, according to the electrical resistivity changes shown in Fig. 1(a). However, the CRSS values at both room temperature and 77 K do not change significantly with annealing temperature, furthermore, all the CRSS values are comparable to those of specimens quenched from 1473 K. Note that no significant change in CRSS is observed also for specimens furnace-cooled from 1273 K (at a rate of 100 K/h). This result is in contrast to an earlier paper [43] on polycrystalline Cr-Co-Ni that reported a 25% yield stress increase in specimens aged at 1273 K for 120 h and furnace-cooled relative to their unaged and water-quenched counterparts despite the aged specimens having a larger grain size (i.e., lower Hall-Petch strengthening).

We also investigated effects of isothermal annealing at 673 K on the CRSS at room temperature both in tension and compression, as shown in Fig. 4(b). We employed 673 K as the isothermal annealing temperature as there is a large change in electrical resistivity at this temperature and the change occurs very gradually (Fig. 1(a)). The dotted line in the figure is the CRSS value obtained in compression for specimens quenched from

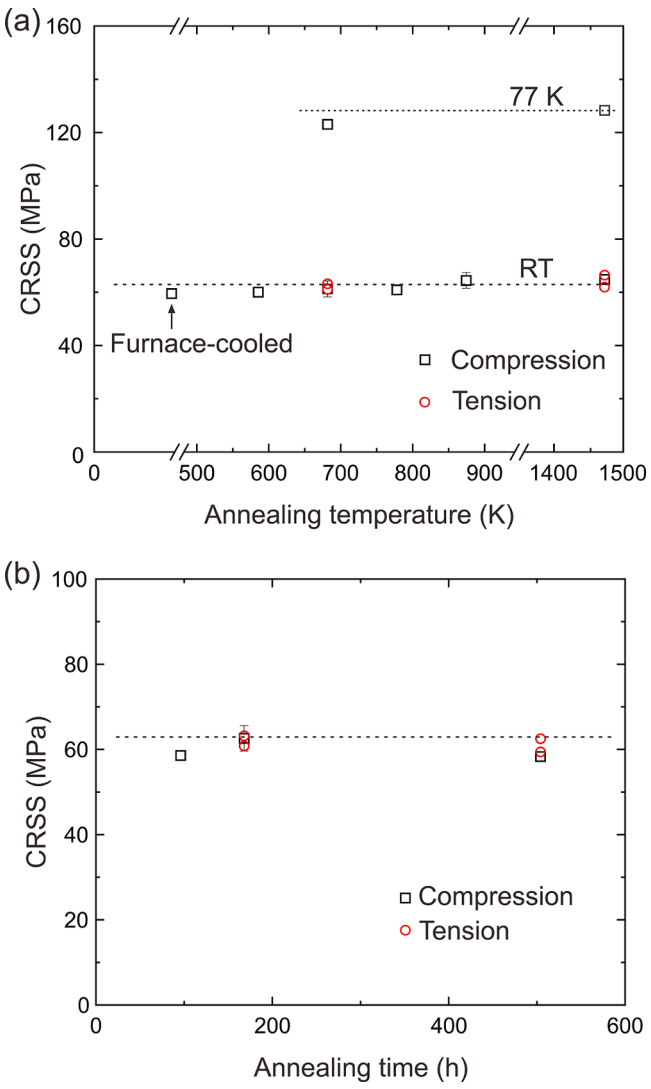

Fig. 4. (a) CRSS values for (111) slip obtained for [$\bar{1}$23]-oriented single crystals of the equiatomic Cr-Co-Ni MEA at room temperature in compression and tension and at 77 K in compression plotted as a function of subsequent annealing temperature (for 168 h) after quenching form 1473 K. (b) CRSS values for (111) slip obtained at room temperature in compression and tension for [$\bar{1}$23]-oriented single crystals of the equiatomic Cr-Co-Ni MEA quenched from 1473 K plotted as a function of isothermal annealing time at 673 K.

1473 K after annealing for 168 h. The CRSS values obtained in compression and tension at room temperature are, again, all comparable with that for specimens quenched from 1473 K, and they do not change significantly with annealing time at 673 K, although the degree of SRO must change gradually but significantly to the highest level after 504 h as indicated by the greater than 4% electrical resistivity increase under these conditions (Fig. 1(a)).

We thus conclude that the degree of SRO does not affect significantly the CRSS value for (111) slip in the equiatomic Cr-Co-Ni MEA. This conclusion is consistent with what is observed for Cu-Al [32] and Cu-Au alloys [18,20] and also for the Cr-Mn-Fe-Co-Ni HEA [46] and Cr-Co-Ni MEA [42], but is in contrast to most theoretical predictions [13,14,39,41,44] and to the report by Zhang et al. [43] that the yield strength increased by 25% due to SRO in polycrystals of Cr-Co-Ni after furnace-cooling from 1273 K.

3.3.2. Dislocation structures

Dislocation structures revealed by bright-field and weak-beam dark-

field imaging in [$\bar{1}$23]-oriented single crystals are shown in Fig. 5(a), (b) for specimens water-quenched from 1473 K, and Fig. 5(d), (e) for specimens water quenched and subsequently annealed at 773 K for 68 h. We selected these two conditions as representatives of the lowest and highest SRO respectively, similar to those used for TEM observations, Figs. 2 and 3. Both specimens were compressed at room temperature to about 3% plastic strain, and a thin foil was cut parallel to the (111) macroscopic slip plane. In both specimens, typical planar arrays of smoothly curved long dislocations are observed on the (111) slip planes in the bright-field images, Fig. 5(a) and (d). Although the dominance of screw dislocations upon SRO strengthening is theoretically predicted [67], no significant change in dislocation alignment along particular orientations was noted after SRO formation in the equiatomic Cr-Co-Ni MEA. The observed planar array of dislocations is consistent with a low stacking fault energy of the alloy, as evident from the large separation distance between paired Shockley partial dislocations in the weak-beam images of Fig. 5(b) and (e). The separation distance between paired Shockley partial dislocations was measured as a function of angle θ between the Burgers vector and line direction of the perfect dislocations in Fig. 5(c) and (f) to deduce the stacking fault energy of the two alloys. Although the dissociation widths in both alloys exhibit scatter, they are in the range of those reported for pure Cu [68], Ag [69] and for the Cr-Mn-Fe-Co-Ni HEA [46,70,71]. On top of that, the magnitude of the scatter is similar for these two alloys (one quenched from 1473 K and the other subsequently annealed at 773 K) and does not change much after annealing at 773 K. This contrasts with what is predicted from theoretical calculation for alloys with SRO, in which a significant variation in dissociation width is predicted in the presence of local SRO [13,14]. From the orientation dependence of dissociation width, we deduced the stacking fault energy of 13.5 mJ/m^2 for the Cr-Co-Ni MEA water-quenched from 1473 K and 13.3 mJ/m^2 for the same alloy subsequently annealed at 773 K for 68 h. This indicates that the stacking fault energy is virtually unchanged with the development of SRO in the equiatomic Cr-Co-Ni MEA. Our finding here is consistent with our

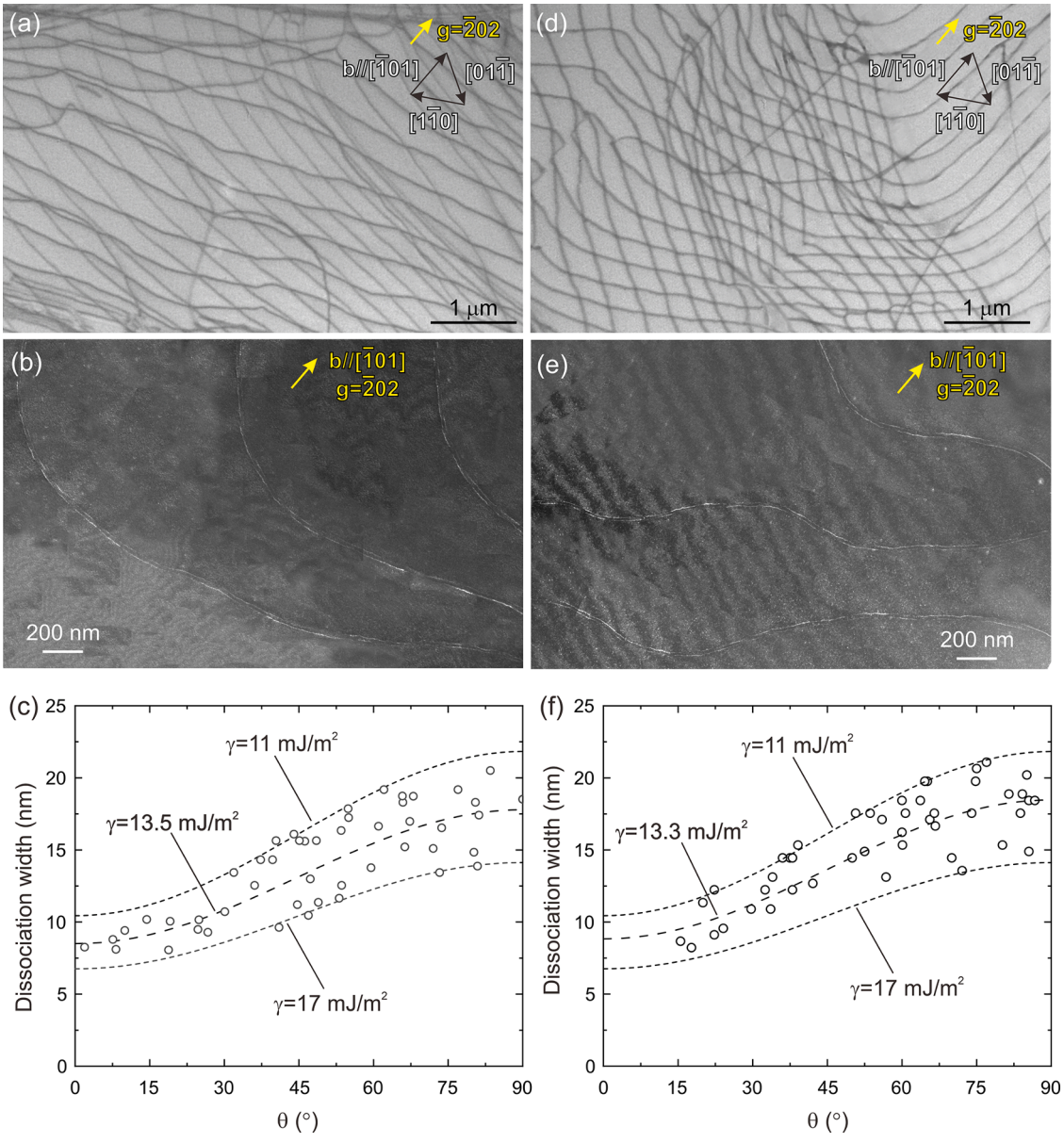

Fig. 5. Dislocation structures reveled by (a), (d) bright-field and (b), (e) weak-beam dark-filed imaging for [$\bar{1}$23]-oriented single crystals (a), (b) water-quenched from 1473 K and (d), (e) subsequently annealed at 773 K for 168 h. Separation distance between paired Shockley partial dislocations were measured as a function of angle θ between the Burgers vector and line direction of the perfect dislocations for [$\bar{1}$23]-oriented single crystals (c) water-quenched from 1473 K and (f) subsequently annealed at 773 K for 168 h.

previous finding in Cr-Mn-Fe-Co-Ni [46] but at odds with the paper by Zhang et al. [43] in which the stacking fault energy of the equiatomic Cr-Co-Ni MEA was reported to increase significantly from 8 mJ/m^2 after water quenching to 23 mJ/m^2 after furnace-cooling from 1273 K and attributed to increased SRO in the latter condition.

3.3.3. *Yield drop, electrical resistivity change and slip localization in tension*

In some dilute FCC alloys, a noticeable yield drop is believed to emerge in the tensile stress-strain curve accompanied by localized (coarse and planar) slip bands as a result of SRO [17,32]. This is believed to be due to the quick dissipation of the SRO-induced high resistance to dislocation motion by the passage of the first several dislocations that destroy SRO on the slip plane, so that subsequent dislocations move on the same slip plane experiencing less resistance, thereby forming coarse slip bands [32]. To check whether this is also the case for the equiatomic Cr-Co-Ni MEA, we investigated the magnitude of yield drop and slip localization behavior with the use of [$\bar{1}$23]-oriented single crystals water-quenched from 1473 K and subsequently annealed at 673 K for 168 or 504 h. The increments in electrical resistivity for the latter two specimens are 3.4 and 4.8%, respectively.

Tensile stress-strain curves obtained at room temperature for these specimens are shown in Fig. 6(a) up to the end of stage I. Yield drop occurs for all specimens but in a rather wide range of plastic strain (usually exceeding several percent of engineering strain) so that the stress-strain curve in stage I exhibits a concave upward shape without a plateau. This is different from the behavior observed for some conventional dilute FCC alloys, in which a sharper yield drop occurs (within a few percent of plastic strain), followed by a plateau stress [17,18,32,33]. In the present study, we define the yield drop as the difference between the upper yield stress and lowest flow stress in stage I. The magnitudes of the yield drop estimated from the tensile stress-strain curves in Fig. 6(a) are 12.11 ± 2.5, 8.83 ± 3.5 and 9.39 ± 2.5 MPa for single crystals water-quenched from 1473 K, and water-quenched and subsequently annealed at 673 K for 168 and 504 h, respectively. The degree of SRO (as determined by the increment in electrical resistivity) does not correlate with the extent of yield drop in the equiatomic Cr-Co-Ni MEA (Fig. 6(b)). This is consistent with the result reported by Büttner and Nembach [18] and Kuhlmann et al. [20] for Cu-Au alloys but is in contrast to what is observed for conventional dilute FCC alloys [17,32].

We also investigated changes in electrical resistivity during tensile deformation in stage I by conducting interrupted tensile tests at room temperature for [$\bar{1}$23]-oriented single crystals water-quenched from 1473 K and subsequently annealed at 673 K for 504 h, as shown in Fig. 6 (c). As in Fig. 1(a), values plotted in Fig. 6(c) are all normalized to the value (ρ_0) of electrical resistivity obtained after quenching from 1473 K. That is why the starting value of electrical resistivity is 1.04 for the specimen subsequently annealed at 673 K for 504 h, while it is 1 for the specimen water-quenched from 1473 K. Because of the dislocations introduced during deformation (and stored in the specimen), the electrical resistivity is generally expected to increase as deformation proceeds. In the equiatomic Cr-Co-Ni MEA, however, the resistivity first decreases, exhibiting a minimum at an engineering strain of 6~7%, followed by an increase at higher strains for both specimens. The strain level for the minimum flow stress almost coincides with that for the minimum electrical resistivity for both specimens. The decrease in electrical resistivity at the minimum is about 3% for the single crystal water-quenched from 1473 K, while it is a bit larger, 4%, for the single crystal subsequently annealed at 673 K for 504 h. The decrease in electrical resistivity following deformation (i.e., by dislocation introduction) together with the decrease in electrical resistivity by low-temperature annealing is usually called the K-effect [22,72]. It is usually thought to be caused by a special atom arrangement of the SRO-type [22] where the decrease in electrical resistivity in the early stages of deformation occurs via the destruction of SRO by the motion of dislocations. If this is the case for the equiatomic Cr-Co-Ni MEA, single crystals water-quenched from 1473 K, as well as those subsequently annealed at 673 K for 504 h, both contain some degree of SRO prior to

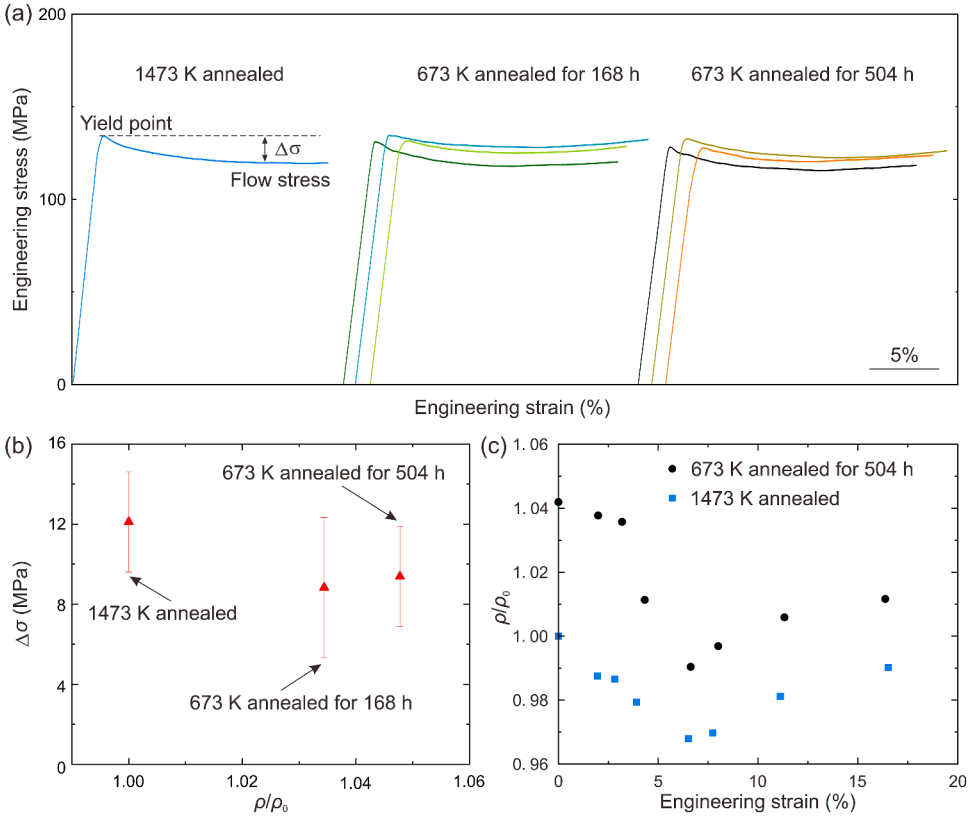

Fig. 6. Tensile stress-strain curves up to the end of stage I obtained at room temperature for [$\bar{1}$23]-oriented single crystals water-quenched from 1473 K and subsequently annealed at 673 K for 168 and 504 h. (b) Magnitude of yield drop measured for these three different specimens from (a). (c) Variations of electrical resistivity for [$\bar{1}$23]-oriented single crystals water-quenched from 1473 K and subsequently annealed at 673 K for 504 h measured as a function of plastic strain in stage I in tensile deformation.

deformation. Additionally, this SRO is destroyed by the motion of dislocations, and the decrease in the degree of SRO is larger for the single crystal subsequently annealed at 673 K for 504 h because of its higher initial degree of SRO. However, the initial degree of SRO in the single crystals water-quenched from 1473 K may not be very high since its electrical resistivity is comparable to that of specimens quenched from the liquid state in which the degree of SRO is expected to be minimized.

We investigated step heights of the deformation markings formed in the very early stages of plasticity by optical and atomic force microscopy to evaluate how the development of SRO affects slip localization behaviors. To that end, [$\bar{1}$23]-oriented single crystals water-quenched from 1473 K as well as those subsequently annealed at 673 K for 504 h were examined, as shown in Fig. 7. The specimen geometry for optical and atomic force microscopy observations is depicted in Fig. S4. The observations were made (1) at a very small strain level (~0.4% plastic strain) corresponding to the peak stress of the upper yield point, and (2) at a strain level corresponding to about 1% additional plastic strain at the same position in both specimens. The densities of slip bands revealed

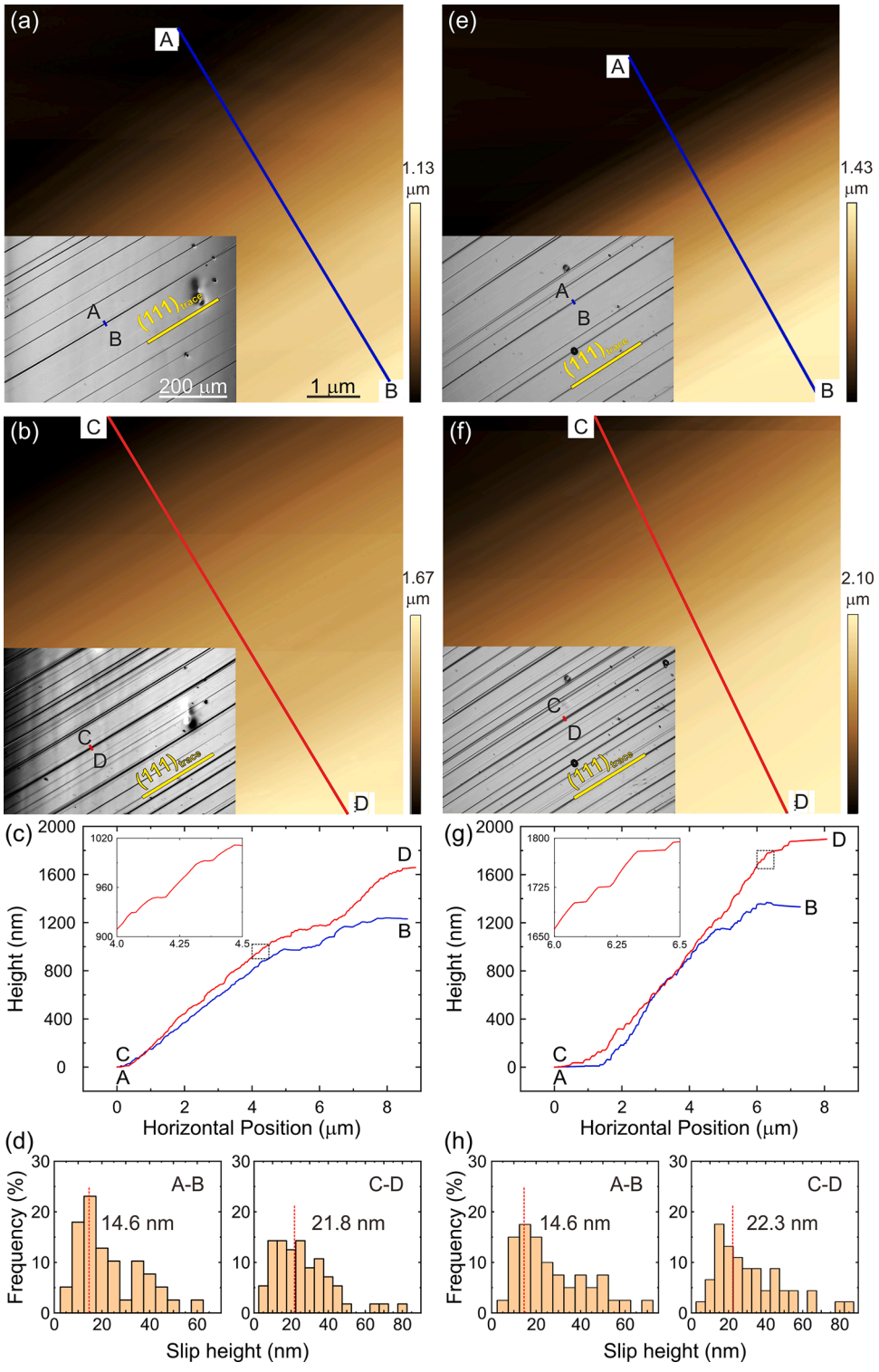

Fig. 7. Deformation markings reveled by optical and atomic force microscopy in the (54$\bar{1}$) surface of [$\bar{1}$23]-oriented single crystals (a), (b) water-quenched from 1473 K and (e), (f) subsequently annealed at 673 K for 504 h (a), (e) at a very small strain level (~0.4% plastic strain) corresponding to the peak stress of upper yielding and (b), (f) at a strain level with about 1% additional plastic strain. Height variation diagrams measure by atomic force microscopy along A-B and C-D and histograms of slip heights formed from the height variation diagrams are shown for (c), (d) [$\bar{1}$23]-oriented single crystals water-quenched from 1473 K and for (g), (h) those subsequently annealed at 673 K for 504 h.

by optical microscopy are almost identical for the two specimens at the same strain levels in spite of the different degrees of SRO. In both specimens, new slip bands are observed to form between existing slip bands as deformation proceeds, in spite of the decreasing flow stress. This clearly indicates that the emergence of yield drop is not necessarily related to the quick decay of the SRO-induced high resistance to dislocation motion by the passage of the first several dislocations during the formation of a new slip band/line [32]. Atomic force microscopy revealed that a slip band optically observed as a single line actually consists of a number of slip steps parallel to (111), as seen in the height variation diagrams of Fig. 7(c) and (g). Comparison of the diagrams along AB and CD in Fig. 7(c) and (g) clearly indicates that, in addition to incremental slip at existing slip lines in the band, widening of the slip band also occurs by forming adjacent slip lines in both specimens. From Fig. 7(c) and (g), histograms of slip heights can be determined, which are plotted in Fig. 7(d) and (h). The averaged slip heights are almost identical for the two specimens at the same strain levels. For both specimens, the average slip height increases from 15 to 22 nm during 1% additional plastic strain in stage I. These average slip heights in the Cr-Co-Ni MEA are comparable to those observed in stage I for FCC alloys with a low stacking fault energy (27 nm for Cu-19 at.% Zn and 24 nm Cu-30 at.% Zn [73]). These results indicate that the development of SRO does not significantly affect the slip localization behavior in the Cr-Co-Ni MEA. This is in contrast to what is believed to occur in the presence of SRO in some conventional dilute FCC alloys [17,32,73,74].

3.3.4. *Deformation at large strain levels in tension*

Fig. 8(a) shows engineering stress-strain curves obtained in tension at room temperature for [$\bar{1}$23]-oriented single crystals of the Cr-Co-Ni MEA: one water-quenched from 1473 K and the other subsequently annealed at 673 K for 504 h. The stress-strain curve for the specimen water-quenched from 1473 K is from our previous study [66] where it was deformed until failure occurred. Two inflection points are evident in the stress-strain curve, following stage II (linear work-hardening). The first inflection point at about 150% strain corresponds to the end of overshooting (i.e., the change in the dominant slip system from the (111)[$\bar{1}$01] primary slip system to the ($\bar{1}\bar{1}$1)[011] conjugate slip system), and the second point corresponds to the change in the dominant deformation mode from ($\bar{1}\bar{1}$1)[011] conjugate slip to (111) [$\bar{2}$11] primary twinning [66]. In this study, the tensile test for the single crystal subsequently annealed at 673 K for 504 h was interrupted at a strain level of 220% immediately after the second inflection point for detailed observations of deformation microstructures. Although the degree of SRO in the two specimens is expected to be significantly different based on their different resistivities, their tensile stress-strain curves are quite similar to each other. The yield stress, length of stage I, the stress and strain levels at which the first and second inflection points occur are all virtually the same for the two specimens despite their different degrees of SRO. This indicates that the deformation behavior does not vary significantly with degree of SRO not only in the early stages of deformation (as described in the previous sections) but also after large strains. In fact, as in the water-quenched single crystal, the second inflection point in the single crystal annealed at 673 K for 504 h also corresponds to the onset of (111) [$\bar{2}$11] primary twinning, Fig. 8(d) and (e). The thickness and volume fraction of twins are virtually the same as those of the single crystal water-quenched from 1473 K (Fig. 8(b) and (c)), when compared at similar strain levels. The true stresses for the onset of twinning are 995 ± 30 MPa for the single crystal water-quenched from

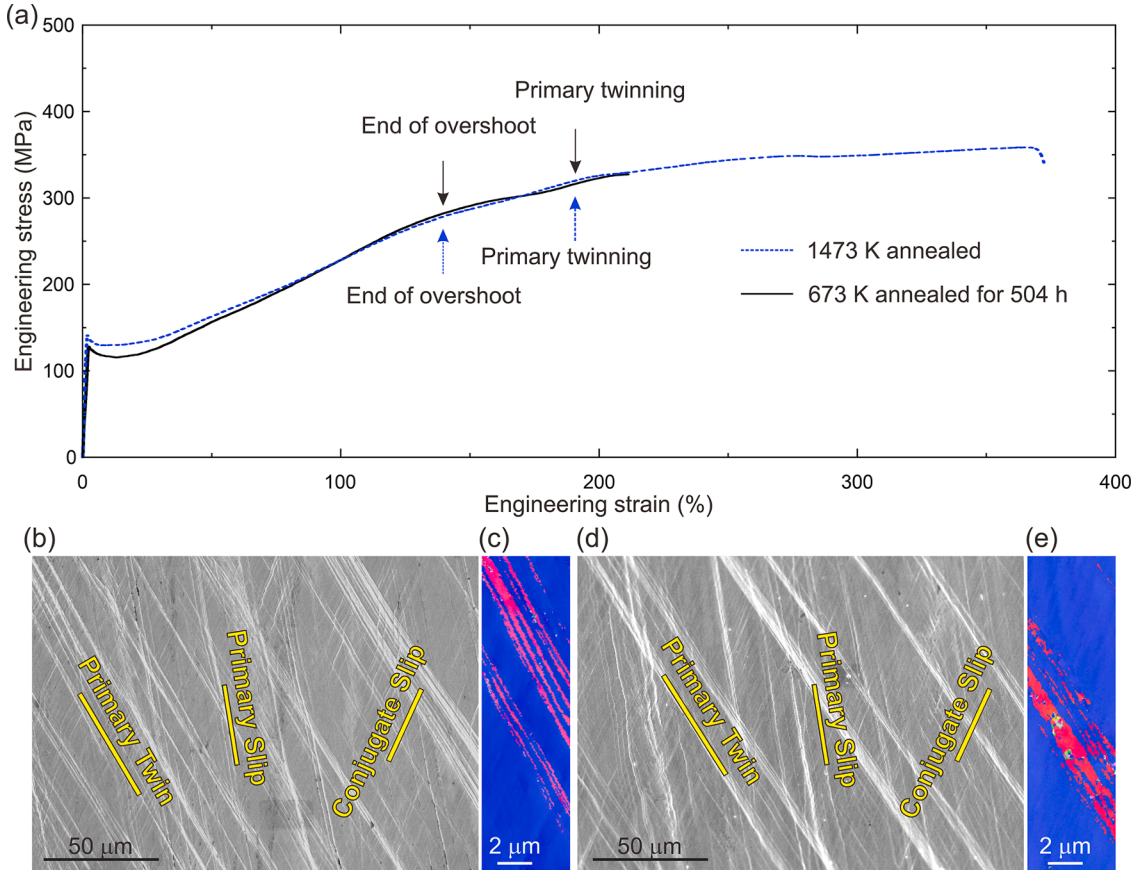

Fig. 8. (a) Tensile stress-strain curves obtained in tension at room temperature for [$\bar{1}$23]-oriented single crystals water-quenched from 1473 K and subsequently annealed at 673 K for 504 h. (b), (d) Optical micrographs and (c), (e) EBSD maps to show deformation twinning are taken from [$\bar{1}$23]-oriented single crystals (b), (c) water-quenched from 1473 K and (d), (e) subsequently annealed at 673 K for 504 h.

1473 K and 991 ± 70 MPa for that subsequently annealed at 673 K for 504 h (these values are considerably higher than the twinning stress (740 ± 45 MPa) for polycrystals in previous study [75], in which deformation twinning initiates at a much lower strain levels). Consequently, the twinning shear stresses calculated using the corresponding Schmid factor (0.409) [66] are also similar, 407 ± 12 MPa and 405 ± 29 MPa. This is a clear indication that the twinning behavior does not vary significantly with the degree of SRO.

4. Discussion

4.1. Evidence for SRO

Using electron diffraction and HAADF-STEM imaging Zhang et al. [43] reported SRO in equiatomic Cr-Co-Ni MEA polycrystals after annealing at 1273 K followed by furnace cooling. They described that SRO in the equiatomic Cr-Co-Ni MEA polycrystals is detected as streaks elongated along the <111> directions [43]. On the other hand, Zhou et al. [37] associated SRO in the equiatomic Cr-Co-Ni MEA with diffuse intensity at the 1/2{113} positions in SAED patterns with the <112> incidence. Here we did not observe streaks along <111> but did observe diffuse intensity at positions of 1/3{422} and 1/2{113} in the SAED patterns for [111] and [112] incidences. However, these diffuse intensities did not change significantly with degree of SRO. Additionally, such diffuse intensities can also be due to other factors such as thin film effects ({111} relrod spiking) and/or surface steps parallel to {111}. The above factors, along with the very small difference in atomic scattering factors of Cr, Co and Ni, make it very difficult to obtain unambiguous evidence for SRO in the Cr-Co-Ni MEA by x-ray and electron diffraction methods.

In contrast, electrical resistivity measurements seem to offer a suitable way to detect SRO in the equiatomic Cr-Co-Ni MEA in a fairly quantitative manner. Recent kinetic Monte-Carlo calculations using potentials generated by neural networks by Du et al. [76] have predicted that the changes in the Warren-Cowley parameters of the equiatomic Cr-Co-Ni MEA upon aging are very similar to the changes in electrical resistivity shown in Fig. 1(a) with the saturated Warren-Cowley parameter α_{Cr-Co} reaching a value of -0.217 at 700 K. Although the degree of SRO is expected to correlate well with changes in electrical resistivity, a linear correlation between the two has yet to be proven. A lattice contraction is predicted to accompany SRO in some MEAs including the equiatomic Cr-Co-Ni MEA by DFT calculations [44]. And, indeed, we observed a decrease in the lattice constant from 0.35666 nm (for samples quenched from 1473 K) to 0.35662 nm (for those subsequently annealed at 673 K for 168 h), and then to 0.35648 nm (for those subsequently annealed at 673 K for 504 h) by our X-ray diffraction. Interestingly, the lattice constant returns to the original value upon re-annealing at 1473 K, consistent with a similar recovery of electrical resistivity. This is further evidence of SRO in the equiatomic Cr-Co-Ni MEA.

4.2. Microstructural evolution accompanying SRO

Some alloys like those in the Ni-Cr [49] and Ni-Mo [77] systems are known to exhibit the so-called K-effect [72] that is believed to be closely related to SRO. The increased electrical resistivity during low-temperature annealing is attributed to the formation of small Ni_3Cr- or Ni_2Cr-like clusters in Ni-Cr alloys [49] and to the formation of SRO of the $L1_2$-type in a Ni-Al-Fe alloy [22]. Theoretical calculations have indicated that the increased resistivity after low-temperature annealing in, for example, Ni-Cr [78] and Ni-Mo [77] alloys, is due to the formation of a local atomic arrangement in which a Cr (or Mo) atom is preferentially surrounded by Ni atoms, i.e., Ni_3Cr cluster of the $L1_2$-type. We postulate that the formation of small Ni_3Cr clusters (or $(Ni,Co)_3Cr$ clusters in the case of the Cr-Co-Ni MEA) of the $L1_2$-type causes (at least partially, that is, in addition to SRO) the increase in electrical resistivity observed after low-temperature annealing in the equiatomic Cr-Co-Ni MEA (Fig. 1(a)). Thermodynamically speaking, the formation of inhomogeneous structure containing small clusters of the $(Ni,Co)_3Cr$ type in CrCoNi is usually described as the precursor to phase separation and precipitation but not SRO states in which a statistically homogeneous structure is assumed. Practically speaking, however, it is very difficult to realize such phase separation (i.e., formation of $L1_2$-$(Ni,Co)_3Cr$ clusters having a "discrete" interface with the FCC matrix) in experiments. As evidence, we note that the TEM microstructure and electrical resistivity after annealing at 773 K for half a year are essentially identical to those after annealing at 773 K for 168 h.

We now estimate from Fig. 1 the size and volume fraction of these small clusters of the $(Ni,Co)_3Cr$-type. The preexponential factor β_0 ($2.85 \times 10^{-10\pm1.7}$ s) is much longer than the mean time for monoatomic jump (i.e., atomic jump to the nearest neighbor site, or the inverse of the lattice vibration frequency) of about$\beta_{mono} = 10^{-13}$ s and can be considered approximately as the cumulative number of atom jumps required for the formation of small clusters with a higher degree of SRO. Then, the ratio $\beta_0/\beta_{mono} \sim 3000$ corresponds to the total number of atoms in each cluster, which indicates a diameter of about 3–4 nm for each cluster if a spherical shape is assumed. If we suppose that the specimen subjected to low temperature annealing in the saturated state consists of the as-quenched matrix with resistivity $\rho_{AQ,}$ plus small clusters with resistivity ρ_{SC}, the total resistivity ρ_{sat} can be expressed by the mean approximation as

$$\frac{\rho_{sat}}{\rho_{AQ}} = (1 - V_{SC}) + \frac{\rho_{SC}}{\rho_{AQ}} V_{SC} \tag{3}$$

where V_{SC} is the volume fraction of the small clusters and

$$\frac{\rho_{sat}}{\rho_{AQ}} = \delta + 1 \tag{4}$$

where δ is the fractional increase of resistivity in Eq. (1). Theoretical calculation has suggested that the residual resistivity of a Ni-Cr alloy changes by $\sim 2 \times 10^{-7}$ Ωm by preferential formation of a Cr-Ni pair from the random state [78]. If the same resistivity change is assumed for the present Cr-Co-Ni alloy, and a value of $\rho_{AQ} = 1.02 \times 10^{-6}$ Ωm [79] is used, $\rho_{SC}/\rho_{AQ}$is calculated to be 1.22. This leads to the relationship $V_{SC} = \delta/0.22$ from which the volume fraction of small clusters is calculated to be $V_{SC} = 0.21$ at $\delta = 0.047$ (i.e., at 673 K, where the saturation resistivity is the highest in the present study). Similarly, the volume fraction of small clusters is calculated to be $V_{SC} = 0.18$ at $\delta = 0.039$ (773 K) and $V_{SC} = 0.12$ at $\delta = 0.027$ (873 K).

The above analyses, though crude, helps us visualize the atomic structures in the equiatomic Cr-Co-Ni MEA as follows. First, when the SRO state is defined by an SRO parameter like Warren-Cowley, the atomic arrangement is implicitly assumed to be uniform everywhere, i.e., the same degree of SRO should be present throughout the specimen. Here, on the other hand, the specimen contains some clusters with higher degree of order of the $(Ni,Co)_3Cr$-type surrounded by a matrix with lower degree of order (the matrix may exhibit SRO in the classical sense). Second, the size of these clusters is about 3–4 nm in diameter and their volume fraction is at most only 0.2. Third, the boundary between the two different regions (that is, between the clusters and matrix) may be diffuse and not discrete, although further study is needed to clarify this. Finally, the small size of clusters with higher degree of order may indicate that these clusters do not grow much in size during isothermal annealing but rather increase in density until the saturation value is reached at the various annealing temperatures. In view of these non-uniform atomic arrangements that are inhomogeneously distributed in the material, and the relatively large cluster sizes of a few nm, it may be better in the future to refer to such atomic structures as "medium-range ordering" rather than short-range ordering as is often the current practice in the HEA/MEA literature. This alternative terminology is an attempt to describe the mixture of nanoscale ordered clusters

inhomogeneously distributed in a matrix that also exhibits SRO.

4.3. Changes in mechanical properties with SRO

In contrast to an earlier report [43] of a remarkable 25% increase in yield strength associated with SRO in polycrystalline, equiatomic Cr-Co-Ni after annealing at 1273 K followed by furnace cooling, here we find essentially no change in the CRSS of single crystals of the equiatomic Cr-Co-Ni subjected to different heat treatments, as well as only a 2% increase in electrical resistivity after furnace cooling (at a rate of 100 K per hour) from 1273 K. A possible reason for this discrepancy may be that Zhang et al. [43] tested large-grained polycrystals (grain sizes of 800 μm and 1000 μm in the water-quenched and aged specimens, respectively). Their relatively small tensile specimens had a thickness of 800 μm, which means that they contained only one grain through the thickness. Unless, by coincidence, the differently heat treated specimens had exactly the same orientation of the through-thickness grains, it is entirely possible that part or all of their yield strength increase (25%) was due to differences in grain orientations. Here, by contrast, our tensile specimens were all oriented for single slip along the $[\bar{1}23]$ loading axis, which allows us to more precisely determine any effect of SRO on CRSS without the confounding effects of different orientations in different gage sections. Inoue et al. [48] reported no measurable change in the yield strength of polycrystalline, equiatomic Cr-Co-Ni after annealing at 973 K for 384 h followed by water quenching. The latter results are understandable based on Fig. 1(a) because the annealing temperature (973 K) they employed is too high to form significant SRO as the increment in electrical resistivity is small (0.5%). Yin et al. [42] reported no measurable change in hardness of polycrystalline, equiatomic Cr-Co-Ni after annealing at 873 K for 384 h, which is consistent with the present results.

The electrical resistivity measurements in the present study show that SRO (and/or ordered clusters) are present in the equiatomic Cr-Co-Ni MEA in the temperature range of 673–873 K with the saturation value of electrical resistivity being higher at lower temperatures (the increment is 2.7% at 873 K and 4.8% at 673 K, see Fig. 1(a)). In spite of changes in electrical resistivity upon annealing in this range, no significant change in the plastic deformation behavior is found for single crystals of the equiatomic Cr-Co-Ni MEA. In the equiatomic Cr-Co-Ni MEA, neither yield strength nor yield drop correlate with the degree of SRO as in Cu-Au [18,20] and Ag-Au [33] polycrystals. This is also the case for the strain localization behavior, dislocation structure and variations in dislocation dissociation width, none of which are significantly affected by the formation of SRO in the equiatomic Cr-Co-Ni MEA. This may mean that even when a finite value of Warren-Cowley parameter is obtained (α_{Cr-Co}= -0.217 at the minimum), changes in atomic arrangement before and after the formation of SRO are not significant enough in the ternary system to significantly affect the dislocation behavior, as discussed in Section 4.2.

5. Conclusions

We investigated the evolution of SRO in the equiatomic Cr-Co-Ni MEA by monitoring changes in electrical resistivity and compared it to changes in X-ray and electron diffraction signals. We also investigated the effects of SRO on the mechanical properties of single crystals of the equiatomic Cr-Co-Ni MEA in tension and in compression at room temperature and liquid nitrogen temperature. Based on the results obtained, the following conclusions can be drawn.

(1) The development of SRO in the Cr-Co-Ni MEA cannot be monitored by simple X-ray and electron diffraction experiments because of the very small difference in atomic scattering factors of the constituent elements. But it can be easily monitored by electrical resistivity measurements.

(2) The electrical resistivity increases gradually and reaches a saturation value during isothermal annealing at a temperature in the range of 673–973 K. While the time required for saturation is shorter at higher temperatures, the saturation value is higher at lower temperatures. This indicates that the degree of SRO is higher at lower temperatures but the kinetics of short-range ordering are slower at lower temperatures.

(3) In spite of changes in electrical resistivity (and the implied changes in degree of SRO) upon annealing at temperatures in the range of 673–973 K, no significant change in the plastic deformation behavior is found at room temperature and at 77 K for single crystals of the equiatomic Cr-Co-Ni MEA. The yield stress as well as the slip localization behavior does not change much as a result of SRO, and the magnitude of yield drop does not correlate with the degree of SRO. The tensile stress-strain curve does not change much with SRO up to high strain levels, giving rise to identical shear stress for the onset of deformation twining at room temperature in specimens with high and low degrees of SRO. The dislocation structure, variations in dislocation dissociation width and stacking fault energy are also all essentially unchanged.

Declaration of Competing Interest

The authors declare that they have no known competing financial interests or personal relationships that could have appeared to influence the work reported in this paper.

Acknowledgments

This work was supported by Grant-in-Aids for Scientific Research on Innovative Areas on High Entropy Alloys through the Grant Nos. JP18H05450 and JP18H05451, in part by JSPS KAKENHI (Grant Nos. JP18H05478, JP19H00824, JP19K22053, JP21H01651, JP21H00140 and JP22H00262), the Elements Strategy Initiative for Structural Materials (ESISM) from the Ministry of Education, Culture, Sports, Science and Technology (MEXT) of Japan (Grant No. JPMXP0112101000), JST CREST (Grant No. JPMJCR1994), and JST Spring (Grant No. JPMJSP2110). Structure refinement of the short-range ordering was supplementally corroborated by the synchrotron radiation experiments at the BL02B1 of SPring-8 with the approval of the Japan Synchrotron Radiation Research Institute (JASRI, Proposal Nos. 2021A1529 and 2022A1391).

Supplementary materials

Supplementary material associated with this article can be found, in the online version, at doi:10.1016/j.actamat.2022.118537.

References

[1] D.B. Miracle, O.N. Senkov, A critical review of high entropy alloys and related concepts, Acta Mater. 122 (2017) 448–511, https://doi.org/10.1016/j.actamat.2016.08.081.
[2] E.P. George, D. Raabe, R.O. Ritchie, High-entropy alloys, Nat. Rev. Mater. 4 (2019) 515–534, https://doi.org/10.1038/s41578-019-0121-4.
[3] Z. Li, S. Zhao, R.O. Ritchie, M.A. Meyers, Mechanical properties of high-entropy alloys with emphasis on face-centered cubic alloys, Prog. Mater. Sci. 102 (2019) 296–345, https://doi.org/10.1016/j.pmatsci.2018.12.003.
[4] E. Ma, Unusual dislocation behavior in high-entropy alloys, Scr. Mater. 181 (2020) 127–133, https://doi.org/10.1016/j.scriptamat.2020.02.021.
[5] E.P. George, W.A. Curtin, C.C. Tasan, High entropy alloys: a focused review of mechanical properties and deformation mechanisms, Acta Mater. 188 (2020) 435–474, https://doi.org/10.1016/j.actamat.2019.12.015.
[6] H. Inui, K. Kishida, L. Li, A.M. Manzoni, S. Haas, U. Glatzel, Uniaxial mechanical properties of face-centered cubic single- and multiphase high-entropy alloys, MRS Bull. 47 (2022) 168–185, https://doi.org/10.1557/S43577-022-00280-Y.
[7] H. Inui, K. Kishida, Z.H. Chen, Recent progress in our understanding of phase stability, atomic structures and mechanical and functional properties of high-

entropy alloys, Mater. Trans. 63 (2022) 394–401, https://doi.org/10.2320/matertrans.MT-M2021234.
[8] W.A. Curtin, S.I. Rao, C. Woodward, Progress and challenges in the theory and modeling of complex concentrated alloys, MRS Bull. 47 (2022) 151–157, https://doi.org/10.1557/s43577-022-00306-5.
[9] N.L. Okamoto, K. Yuge, K. Tanaka, H. Inui, E.P. George, Atomic displacement in the CrMnFeCoNi high-entropy alloy-a scaling factor to predict solid solution strengthening, AIP Adv. 6 (2016), 125008, https://doi.org/10.1063/1.4971371.
[10] Y.Y. Zhao, Z.F. Lei, Z.P. Lu, J.C. Huang, T.G. Nieh, A simplified model connecting lattice distortion with friction stress of Nb-based equiatomic high-entropy alloys, Mater. Res. Lett. 7 (2019) 340–346, https://doi.org/10.1080/21663831.2019.1610105.
[11] A. Tamm, A. Aabloo, M. Klintenberg, M. Stocks, A. Caro, Atomic-scale properties of Ni-based FCC ternary, and quaternary alloys, Acta Mater. 99 (2015) 307–312, https://doi.org/10.1016/j.actamat.2015.08.015.
[12] Y. Rao, W.A. Curtin, Analytical models of short-range order in FCC and BCC alloys, Acta Mater. 226 (2022), 117621, https://doi.org/10.1016/j.actamat.2022.117621.
[13] J. Ding, Q. Yu, M. Asta, R.O. Ritchie, Tunable stacking fault energies by tailoring local chemical order in CrCoNi medium-entropy alloys, Proc. Natl. Acad. Sci. U.S.A. 115 (2018) 8919–8924, https://doi.org/10.1073/pnas.1808660115.
[14] Q.J. Li, H. Sheng, E. Ma, Strengthening in multi-principal element alloys with local-chemical-order roughened dislocation pathways, Nat. Commun. 10 (2019) 1–11, https://doi.org/10.1038/s41467-019-11464-7.
[15] A.C. Damask, Some resistivity effects of short-range order in α brass, J. Appl. Phys. 27 (1956) 610–616, https://doi.org/10.1063/1.1722441.
[16] R.G. Davies, R.W. Cahn, Short range order in aluminium bronze, Acta Metall. 10 (1962) 170–171, https://doi.org/10.1016/0001-6160(62)90062-7.
[17] R.O. Scattergood, M.B. Bever, The relation of short-range order to the deformation behaviour of copper-rich copper-aluminium alloys, Philos. Mag. 22 (1970) 501–514, https://doi.org/10.1080/14786437008225840.
[18] N. Büttner, E. Nembach, On short-range order hardening in Cu-10 at.% Au, Acta Metall. 30 (1982) 83–86, https://doi.org/10.1016/0001-6160(82)90047-5.
[19] W. Pfeiler, Investigation of short-range order by electrical resistivity measurement, Acta Metall. 36 (1988) 2417–2434, https://doi.org/10.1016/0001-6160(88)90192-7.
[20] O. Kuhlmann, H. Rösner, E. Nembach, The effects of order on the critical resolved shear stress of Cu-10 at.% Au single crystals, Acta Mater. 45 (1997) 3319–3326, https://doi.org/10.1016/S1359-6454(97)82885-6.
[21] V.G. Gavriljuk, B.D. Shanina, H. Berns, On the correlation between electron structure and short range atomic order in iron-based alloys, Acta Mater. 48 (2000) 3879–3893, https://doi.org/10.1016/S1359-6454(00)00192-0.
[22] Y. Wang, D. Jiang, W. Yu, S. Huang, D. Wu, Y. Xu, X. Yang, Short-range ordering in a commercial Ni-Cr-Al-Fe precision resistance alloy, Mater. Des. 181 (2019) 1–9, https://doi.org/10.1016/j.matdes.2019.107981.
[23] A. Marucco, B. Nath, Effects of ordering on the properties of Ni-Cr alloys, J. Mater. Sci. 23 (1988) 2107–2114.
[24] A. Marucco, Atomic ordering and α'-Cr phase precipitation in long-term aged Ni_3Cr and Ni_2Cr alloys, J. Mater. Sci. 30 (1995) 4188–4194.
[25] A. Taylor, K.G. Hinton, A study of order disorder and precipitation phenomena in nickel chromium alloys, J. Inst. Met. 81 (1952) 169–180.
[26] N.R. Dudova, R.O. Kaibyshev, V.A. Valitov, Short-range ordering and the abnormal mechanical properties of a Ni-20% Cr alloy, Phys. Met. Metallogr. 108 (2009) 625–633, https://doi.org/10.1134/S0031918X0912014X, 2009 1086.
[27] W. Wagner, R. Poerschke, H. Wollenberger, Dependence of electrical resistivity on the degree of short range order in a nickel-copper alloy, Philos. Mag. B 43 (1981) 345–355, https://doi.org/10.1080/13642818108221904.
[28] P. Cenedese, F. Bley, S. Lefebvre, Diffuse scattering in disordered ternary alloys: neutron measurements of local order in a stainless steel $Fe_{0.56}Cr_{0.21}Ni_{0.23}$, Acta Crystallogr. Sect. A 40 (1984) 228–240, https://doi.org/10.1107/S0108767384000489.
[29] A.Z. Menshikov, C. Dimitrov, A.E. Teplykh, Local atomic redistribution under irradiation in γ - NiFeCr alloys, J. Phys. III 7 (1997) 1899–1908, https://doi.org/10.1051/jp3:1997231.
[30] J.C. Fisher, On the strength of solid solution alloys, Acta Metall. 2 (1954) 9–10, https://doi.org/10.1016/0001-6160(54)90087-5.
[31] P.A. Flinn, Solute hardening of close-packed solid solutions, Acta Metall. 6 (1958) 631–635, https://doi.org/10.1016/0001-6160(58)90156-1.
[32] J.B. Cohen, M.E. Fine, Some aspects of short-range order, J. Phys. Radium 23 (1962) 749–762, https://doi.org/10.1051/jphysrad:019620023010074901.
[33] J.J. Svitak, R.M. Asimow, Solid-solution strenthening in the Ag-Au system, Trans. Met. Soc. AIME 245 (1969) 209–212.
[34] S. Patu, R.J. Arsenault, Strengthening due to non-random solid solutions, Mater. Sci. Eng. A 194 (1995) 121–128, https://doi.org/10.1016/0921-5093(94)09674-0.
[35] F.X. Zhang, S. Zhao, K. Jin, H. Xue, G. Velisa, H. Bei, R. Huang, J.Y.P. Ko, D. C. Pagan, J.C. Neuefeind, W.J. Weber, Y. Zhang, Local structure and short-range order in a NiCoCr solid solution alloy, Phys. Rev. Lett. 118 (2017) 1–6, https://doi.org/10.1103/PhysRevLett.118.205501.
[36] K. Yuge, S. Ohta, Microscopic geometry rules ordering tendency for multicomponent disordered alloys, J. Phys. Soc. Jpn. 88 (2019) 1–6, https://doi.org/10.7566/JPSJ.88.054803.
[37] L. Zhou, Q. Wang, J. Wang, X. Chen, P. Jiang, H. Zhou, F. Yuan, X. Wu, Z. Cheng, E. Ma, Atomic-scale evidence of chemical short-range order in CrCoNi medium-entropy alloy, Acta Mater. 224 (2022) 16–18, https://doi.org/10.1016/j.actamat.2021.117490.
[38] H. Tanimoto, R. Hozumi, M. Kawamura, Electrical resistivity and short-range order in rapid-quenched CrMnFeCoNi high-entropy alloy, J. Alloy. Compd. 896 (2022), 163059, https://doi.org/10.1016/j.jallcom.2021.163059.
[39] X. Yang, Y. Xi, C. He, H. Chen, X. Zhang, S.T. Tu, Chemical short-range order strengthening mechanism in CoCrNi medium-entropy alloy under nanoindentation, Scr. Mater. 209 (2022), 114364, https://doi.org/10.1016/j.scriptamat.2021.114364.
[40] B. Schönfeld, C.R. Sax, J. Zemp, M. Engelke, P. Boesecke, T. Kresse, T. Boll, T. Al-Kassab, O.E. Peil, A.V. Ruban, Local order in Cr-Fe-Co-Ni: experiment and electronic structure calculations, Phys. Rev. B (2019) 99, https://doi.org/10.1103/PhysRevB.99.014206.
[41] F.H. Cao, Y.J. Wang, L.H. Dai, Novel atomic-scale mechanism of incipient plasticity in a chemically complex CrCoNi medium-entropy alloy associated with inhomogeneity in local chemical environment, Acta Mater. 194 (2020) 283–294, https://doi.org/10.1016/j.actamat.2020.05.042.
[42] B. Yin, S. Yoshida, N. Tsuji, W.A. Curtin, Yield strength and misfit volumes of NiCoCr and implications for short-range-order, Nat. Commun. 11 (2020) 2507, https://doi.org/10.1038/s41467-020-16083-1.
[43] R. Zhang, S. Zhao, J. Ding, Y. Chong, T. Jia, C. Ophus, M. Asta, R.O. Ritchie, A. M. Minor, Short-range order and its impact on the CrCoNi medium-entropy alloy, Nature 581 (2020) 283–287, https://doi.org/10.1038/s41586-020-2275-z.
[44] W.R. Jian, Z. Xie, S. Xu, Y. Su, X. Yao, I.J. Beyerlein, Effects of lattice distortion and chemical short-range order on the mechanisms of deformation in medium entropy alloy CoCrNi, Acta Mater. 199 (2020) 352–369, https://doi.org/10.1016/j.actamat.2020.08.044.
[45] J.B. Seol, J.W. Bae, J.G. Kim, H. Sung, Z. Li, H.H. Lee, S.H. Shim, J.H. Jang, W. S. Ko, S.I. Hong, H.S. Kim, Short-range order strengthening in boron-doped high-entropy alloys for cryogenic applications, Acta Mater. 194 (2020) 366–377, https://doi.org/10.1016/j.actamat.2020.04.052.
[46] D. Zhou, Z. Chen, K. Ehara, K. Nitsu, K. Tanaka, H. Inui, Effects of annealing on hardness, yield strength and dislocation structure in single crystals of the equiatomic Cr-Mn-Fe-Co-Ni high entropy alloy, Scr. Mater. 191 (2021) 173–178, https://doi.org/10.1016/j.scriptamat.2020.09.039.
[47] N. Hanasaki, M. Oda, K. Niitsu, K. Ehara, H. Murakawa, H. Sakai, H. Nitani, H. Abe, H. Sagayama, H. Uetsuka, T. Karube, H. Inui, Element dependence of local disorder in medium-entropy alloy CrCoNi, AIP Adv. 11 (2021), 125216, https://doi.org/10.1063/5.0072766.
[48] K. Inoue, S. Yoshida, N. Tsuji, Direct observation of local chemical ordering in a few nanometer range in CoCrNi medium-entropy alloy by atom probe tomography and its impact on mechanical properties, Phys. Rev. Mater. 5 (2021) 1–7, https://doi.org/10.1103/PhysRevMaterials.5.085007.
[49] A.M. Rana, A.F. Khan, A. Abbas, M.I. Ansari, Electrical resistivity behavior in Ni-25 at.% Cr alloy, Mater. Chem. Phys. 80 (2003) 228–231, https://doi.org/10.1016/S0254-0584(02)00468-6.
[50] A.Y. Volkov, A.E. Kostina, E.G. Volkova, O.S. Novikova, B.D. Antonov, Microstructure and physicomechanical properties of a Cu-8 at % Pd Alloy, Phys. Met. Metallogr. 118 (2017) 1236–1246, https://doi.org/10.1134/S0031918X1712016X.
[51] M. Vaidya, S. Trubel, B.S. Murty, G. Wilde, S.V. Divinski, Ni tracer diffusion in CoCrFeNi and CoCrFeMnNi high entropy alloys, J. Alloy. Compd. 688 (2016) 994–1001, https://doi.org/10.1016/j.jallcom.2016.07.239.
[52] M. Vaidya, K.G. Pradeep, B.S. Murty, G. Wilde, S.V. Divinski, Bulk tracer diffusion in CoCrFeNi and CoCrFeMnNi high entropy alloys, Acta Mater. 146 (2018) 211–224, https://doi.org/10.1016/j.actamat.2017.12.052.
[53] D. Gaertner, J. Kottke, Y. Chumlyakov, F. Hergemöller, G. Wilde, S.V. Divinski, Tracer diffusion in single crystalline CoCrFeNi and CoCrFeMnNi high-entropy alloys: kinetic hints towards a low-temperature phase instability of the solid-solution? Scr. Mater. 187 (2020) 57–62, https://doi.org/10.1016/j.scriptamat.2020.05.060.
[54] C. Niu, A.J. Zaddach, A.A. Oni, X. Sang, J.W. Hurt, J.M. Lebeau, C.C. Koch, D. L. Irving, Spin-driven ordering of Cr in the equiatomic high entropy alloy NiFeCrCo, Appl. Phys. Lett. (2015) 106, https://doi.org/10.1063/1.4918996.
[55] T. Fukushima, H. Katayama-Yoshida, K. Sato, M. Ogura, R. Zeller, P.H. Dederichs, Local energies and energy fluctuations - applied to the high entropy alloy CrFeCoNi, J. Phys. Soc. Jpn. 86 (2017) 1–7, https://doi.org/10.7566/JPSJ.86.114704.
[56] Y.S. Kim, W.Y. Maeng, S.S. Kim, Effect of short-range ordering on stress corrosion cracking susceptibility of Alloy 600 studied by electron and neutron diffraction, Acta Mater. 83 (2015) 507–515, https://doi.org/10.1016/j.actamat.2014.10.009.
[57] X. Chen, Q. Wang, Z. Cheng, M. Zhu, H. Zhou, P. Jiang, L. Zhou, Q. Xue, F. Yuan, J. Zhu, X. Wu, E. Ma, Direct observation of chemical short-range order in a medium-entropy alloy, Nature 592 (2021) 712–716, https://doi.org/10.1038/s41586-021-03428-z.
[58] J. Wang, P. Jiang, F. Yuan, X. Wu, Chemical medium-range order in a medium-entropy alloy, Nat. Commun. 13 (2022) 1–6, https://doi.org/10.1038/s41467-022-28687-w.
[59] D.W. Pashley, M.J. Stowell, Electron microscopy and diffraction of twinned structures in evaporated films of gold, Philos. Mag. 8 (1963) 1605–1632, https://doi.org/10.1080/14786436308207327.
[60] D. Cherns, Direct resolution of surface atomic steps by transmission electron microscopy, Philos. Mag. 30 (1974) 549–556, https://doi.org/10.1080/14786439808206580.
[61] D. Cherns, The surface structure of (111) gold films sputtered in the high voltage electron microscope a theoretical model, Philos. Mag. 36 (1977) 1429–1444, https://doi.org/10.1080/14786437708238526.

[62] J.C. Heyraud, J.J. Métois, Anomalous 1/3 422 diffraction spots from {111} flat gold crystallites: (111) surface reconstruction and moiré fringes between the surface and the bulk, Surf. Sci. 100 (1980) 519–528, https://doi.org/10.1016/0039-6028(80)90419-7.
[63] J. Reyes-Gasga, A. Gómez-Rodríguez, X. Gao, M. José-Yacamán, On the interpretation of the forbidden spots observed in the electron diffraction patterns of flat Au triangular nanoparticles, Ultramicroscopy 108 (2008) 929–936, https://doi.org/10.1016/j.ultramic.2008.03.005.
[64] C. Miller, R. Field, M. Kaufman, The presence of higher-order laue zone intensities and the relrod effect in cubic metals in the transmission electron microscope, Microsc. Microanal. 21 (2015) 1665–1666, https://doi.org/10.1017/s1431927615009101.
[65] C. Fernando-Marquez, G. Mondragón-Galicia, L. Bazán-Díaz, J. Reyes-Gasga, Particle size and convergent electron diffraction patterns of triangular prismatic gold nanoparticles, Rev. Mex. Fís. 67 (2021) 1–8, https://doi.org/10.31349/revmexfis.67.041005.
[66] L. Li, Z. Chen, S. Kuroiwa, M. Ito, K. Kishida, H. Inui, E.P. George, Tensile and compressive plastic deformation behavior of medium-entropy Cr-Co-Ni single crystals from cryogenic to elevated temperatures, Int. J. Plast. 148 (2022), 103144, https://doi.org/10.1016/J.IJPLAS.2021.103144.
[67] E. Antillon, C. Woodward, S.I. Rao, B. Akdim, T.A. Parthasarathy, Chemical short range order strengthening in a model FCC high entropy alloy, Acta Mater. 190 (2020) 29–42, https://doi.org/10.1016/j.actamat.2020.02.041.
[68] W.M. Stobbs, C.H. Sworn, The weak beam technique as applied to the determination of the stacking-fault energy of copper, Philos. Mag. 24 (1971) 1365–1381, https://doi.org/10.1080/14786437108217418.
[69] D.J.H. Cockayne, M.L. Jenkins, I.L.F. Ray, The measurement of stacking-fault energies of pure face-centred cubic metals, Philos. Mag. 24 (1971) 1383–1392, https://doi.org/10.1080/14786437108217419.
[70] N.L. Okamoto, S. Fujimoto, Y. Kambara, M. Kawamura, Z.M.T. Chen, H. Matsunoshita, K. Tanaka, H. Inui, E.P. George, Size effect, critical resolved shear stress, stacking fault energy, and solid solution strengthening in the CrMnFeCoNi high-entropy alloy, Sci. Rep. 6 (2016) 35863.
[71] M. Kawamura, M. Asakura, N.L. Okamoto, K. Kishida, H. Inui, E.P. George, Plastic deformation of single crystals of the equiatomic Cr−Mn−Fe−Co−Ni high-entropy alloy in tension and compression from 10 K to 1273 K, Acta Mater. 203 (2021), 116454, https://doi.org/10.1016/j.actamat.2020.10.073.
[72] H. Thomas, Über Widerstandslegierungen, Z. Phys. 129 (1951) 219–232, https://doi.org/10.1007/BF01333398.
[73] H. Neuhäuser, F.R.N. Nabarro, Slip-line formation and collective dislocation motion, in: Dislocations Solids, 6, North-Holland, 1983, pp. 319–440.
[74] J. Plessing, C. Achmus, H. Neuhäuser, B. Schönfeld, G. Kostorz, Short-range order and the mode of slip in concentrated Cu-based alloys, Int. J. Mater. Res. 88 (1997) 630–635, https://doi.org/10.3139/ijmr-1997-0119.
[75] G. Laplanche, A. Kostka, C. Reinhart, J. Hunfeld, G. Eggeler, E.P. George, Reasons for the superior mechanical properties of medium-entropy CrCoNi compared to high-entropy CrMnFeCoNi, Acta Mater. 128 (2017) 292–303, https://doi.org/10.1016/j.actamat.2017.02.036.
[76] J.P. Du, P. Yu, S. Shinzato, F. Meng, Y. Sato, Y.G. Li, Y.W. Fan, S. Ogata, Chemical domain structure and its formation kinetics in CrCoNi medium-entropy alloy, Acta Mater. 240 (2022), 118314, https://doi.org/10.1016/j.actamat.2022.118314.
[77] D.M.C. Nicholson, R.H. Brown, Electrical resistivity of $Ni_{0.8}Mo_{0.2}$: explanation of anomalous behavior in short-range ordered alloys, Phys. Rev. Lett. 70 (1993) 3311–3314, https://doi.org/10.1103/PhysRevLett.70.3311.
[78] S. Lowitzer, D. Ködderitzsch, H. Ebert, P.R. Tulip, A. Marmodoro, J.B. Staunton, An ab initio investigation of how residual resistivity can decrease when an alloy is deformed, EPL (2010) 92, https://doi.org/10.1209/0295-5075/92/37009.
[79] K. Jin, B.C. Sales, G.M. Stocks, G.D. Samolyuk, M. Daene, W.J. Weber, Y. Zhang, H. Bei, Tailoring the physical properties of Ni-based single-phase equiatomic alloys by modifying the chemical complexity, Sci. Rep. 6 (2016) 1–10, https://doi.org/10.1038/srep20159.